Structure of the flavocytochrome C sulfide dehydrogenase associated with the copper-binding protein CopC from the haloalkaliphilic sulfuroxidizing bacterium thioalkalivibrio paradoxus ArH 1

Osipov, Eugeny M.; Lilina, Anastasia V.; Tsallagov, Stanislav I.; Safonova, Tatyana N.; Sorokin, Dimitry Y.; Tikhonova, Tamara V.; Popova, Vladimir O.

DOI
10.1107/S2059798318005648

Publication date
2018

Document Version
Final published version

Published in
Acta Crystallographica Section D: Structural Biology

STRUCTURAL BIOLOGY
ISSN 2059-7983

Structure of the flavocytochrome *c* sulfide dehydrogenase associated with the copper-binding protein CopC from the haloalkaliphilic sulfur-oxidizing bacterium *Thioalkalivibrio paradoxus* ARh 1

Received 5 January 2018
Accepted 10 April 2018

Edited by Z. S. Derewenda, University of Virginia, USA

Keywords: flavocytochrome *c* sulfide dehydrogenase; protein–protein complex; X-ray structure; copper-binding protein; CopC; *Thioalkalivibrio paradoxus*.

PDB reference: complex between flavocytochrome *c* sulfide dehydrogenase and the copper-binding protein CopC from *T. paradoxus*, 5n1t

Supporting information: this article has supporting information at journals.iucr.org/d

Eugeny M. Osipov,[a]* Anastasia V. Lilina,[a] Stanislav I. Tsallagov,[a] Tatyana N. Safonova,[a] Dimitry Y. Sorokin,[a,b] Tamara V. Tikhonova[a] and Vladimir O. Popov[a,c]

[a]Research Center of Biotechnology of the Russian Academy of Sciences, 33 Leninsky Avenue, Building 2, Moscow 119071, Russian Federation, [b]Department of Biotechnology, Delft University of Technology, Delft, The Netherlands, and [c]Kurchatov Complex of NBICS-Technologies, National Research Centre 'Kurchatov Institute', Moscow, Russian Federation. *Correspondence e-mail: e.m.osipov@gmail.com

Flavocytochrome *c* sulfide dehydrogenase from *Thioalkalivibrio paradoxus* (*Tp*FCC) is a heterodimeric protein consisting of flavin- and monohaem *c*-binding subunits. *Tp*FCC was co-purified and co-crystallized with the dimeric copper-binding protein *Tp*CopC. The structure of the *Tp*FCC–$(TpCopC)_2$ complex was determined by X-ray diffraction at 2.6 Å resolution. The flavin-binding subunit of *Tp*FCC is structurally similar to those determined previously, and the structure of the haem-binding subunit is similar to that of the N-terminal domain of dihaem FCCs. According to classification based on amino-acid sequence, *Tp*CopC belongs to a high-affinity CopC subfamily characterized by the presence of a conserved His1-Xxx-His3 motif at the N-terminus. Apparently, a unique α-helix which is present in each monomer of *Tp*CopC at the interface with *Tp*FCC plays a key role in complex formation. The structure of the copper-binding site in *Tp*CopC is similar to those in other known CopC structures. His3 is not involved in binding to the copper ion and is 6–7 Å away from this ion. Therefore, the His1-Xxx-His3 motif cannot be considered to be a key factor in the high affinity of CopC for copper(II) ions. It is suggested that the *Tp*FCC–$(TpCopC)_2$ heterotetramer may be a component of a large periplasmic complex that is responsible for thiocyanate metabolism.

1. Introduction

Flavocytochrome *c* sulfide dehydrogenase (FCC) is one of the central enzymes of oxidative sulfur metabolism in sulfur-oxidizing bacteria (Fukumori & Yamanaka, 1979). This enzyme catalyzes the oxidation of sulfide and polysulfide ions to zero-valent sulfur accompanied by electron transfer to cytochrome *c*. The catalytically active form of the enzyme is a noncovalently bound heterodimer composed of a flavin-binding subunit (~45 kDa) and a monohaem (~10 kDa; Visser *et al.*, 1997; Kostanjevecki *et al.*, 2000) or dihaem (~25 kDa; Fukumori & Yamanaka, 1979; Chen *et al.*, 1994; Hirano *et al.*, 2012) cytochrome subunit. The flavin-binding subunit of FCC contains a covalently bound flavin adenine dinucleotide (FAD) molecule attached by a thioether bond.

The flavin-binding subunit of FCC has a similar fold to that of sulfide:quinone oxidoreductase (SQR; Shahak & Hauska, 2008). Like FCC, the latter enzyme oxidizes sulfide to elemental sulfur and contains an FAD molecule. However,

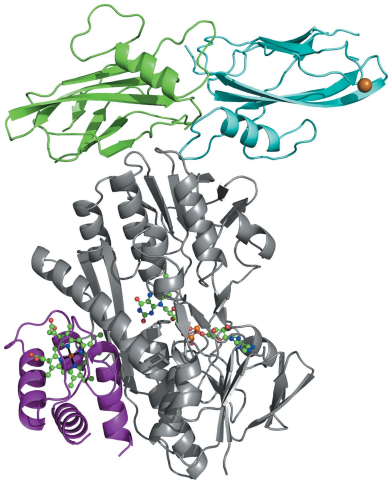

unlike FCC, SQR is a membrane protein that lacks a cytochrome subunit and catalyzes electron transfer from FAD to the quinone pool in the cytoplasmic membrane. In SQR the FAD is bound noncovalently because this enzyme does not have a cysteine residue that is involved in a thioether bond to FAD as in FCC.

The structures of FCCs from two anoxygenic purple sulfur bacteria, *Allochromatium vinosum* (*Av*FCC; Chen *et al.*, 1994) and *Thermochromatium tepidum* (*Tt*FCC; Hirano *et al.*, 2012), and the structures of three SQRs from the hyperthermophilic bacterium *Aquifex aeolicus* (Marcia *et al.*, 2009), the thermoacidophilic sulfur-oxidizing γ-proteobacterium *Acidithiobacillus ferrooxidans* (Cherney *et al.*, 2010, 2012) and the hyperthermophilic acidophilic sulfur-oxidizing archaeon *Acidianus ambivalens* (Brito *et al.*, 2009) have been determined by X-ray crystallography. A pair of active-site conserved redox-active cysteine residues in FCC and SQR located on the *re* side of the isoalloxazine ring of FAD are involved in the oxidation of sulfide ions accompanied by electron transfer to the FAD. The successive oxidation of several sulfide ions leads to elongation of the polysulfide chain between the catalytic cysteines. The following intermediates in this reaction were found by X-ray crystallography: a disulfur molecule S_2 between the catalytic cysteine residues in *Tt*FCC (Hirano *et al.*, 2012) and an S_8 molecule in SQR from *A. aeolicus* (Marcia *et al.*, 2009). Consecutive nucleophilic attacks of new sulfide molecules finally result in release of the polysulfide molecule for stereochemical reasons and restoration of the disulfide bridge in the active site (Brito *et al.*, 2009). The electrons that are released upon sulfide oxidation are transferred from FAD to quinone in SQR or to haem *c* in the cytochrome subunit in FCC. In SQR, quinone is located in the hydrophobic pocket at a distance of 3 Å from FAD, resulting in direct electron transfer. In FCC, the distance between FAD and haem *c* is ∼9 Å. It is assumed that electron transfer from FAD to the haem is mediated by the tryptophan, threonine and tyrosine residues of the flavoprotein subunit located close to the haem group (Chen *et al.*, 1994).

The Gram-negative sulfur-oxidizing γ-proteobacteria of the genus *Thioalkalivibrio* are haloalkaliphilic obligate autotrophs that naturally occur in alkaline (soda) lakes in Africa, Central Asia and North America (Sorokin *et al.*, 2002, 2010, 2014; Grant & Sorokin, 2011). The microbial communities in these lakes have adapted to extreme conditions such as alkaline pH (up to pH 11) and high salinity (up to 4 *M* Na^+). The oxidation of reduced sulfur compounds, such as thiosulfate, sulfide, polysulfide and molecular sulfur, is the main source of energy for the lithoautotrophic microbial communities in soda lakes (Sorokin *et al.*, 2014). Ten out of 85 strains of *Thioalkalivibrio* isolated from soda lakes can grow with thiocyanate (SCN^-) as a the sole energy source (Sorokin *et al.*, 2013). The genome of one of these strains, *T. paradoxus* ARh 1 (Berben *et al.*, 2015), contains five copies of gene clusters that encode proteins homologous to FCC. The amino-acid sequence identity between the flavin-binding subunits encoded by the different copies of the FCC gene is up to 73%. Only one of these five copies corresponds to a dihaem variant, while the other four are monohaem variants. The goal of this work is to study the structure of the monohaem FCC from *T. paradoxus* ARh 1 (*Tp*FCC; NCBI accession Nos. WP_006748977 and WP_006748978 for the cytochrome and flavin-binding subunits, respectively) synthesized during bacterial growth with thiocyanate in the presence of copper ions.

In all steps, FCC was co-purified and then co-crystallized with a protein of the CopC family (copper-resistance protein). CopC proteins can bind copper(I) and copper(II) ions with high affinity ($10^{-7} \geq K_d \geq 10^{-13}$ *M* and $10^{-10} \geq K_d \geq 10^{-17}$ *M*, respectively; Zhang *et al.*, 2006; Wijekoon *et al.*, 2015). The CopC gene is located either in the operon encoding the copper-resistance proteins CopABCDERS or, together with CopD, near the genes for multicopper oxidases (Lawton *et al.*, 2016). It is hypothesized that in the latter case CopC acts as a copper chaperone facilitating the incorporation of copper ions into the active site of folded multicopper oxidases (Lawton *et al.*, 2016). Based on an analysis of amino-acid sequences, the proteins of the CopC family have recently been classified into several subfamilies according to their ability to bind copper ions (Lawton *et al.*, 2016): C_{1-1} CopCs containing copper(I)- and copper(II)-binding sites, C_{1-0} CopCs containing one copper(I)-binding site, C_{0-1} CopCs containing one copper(II)-binding site, C_{0-2} CopCs containing one high-affinity copper(II)-binding site (high affinity means that the binding of copper ion is two orders stronger compared with the proteins of the C_{0-1} subfamily) and C_{0-0} CopCs, which do not bind copper ions. The structures of CopCs from *Methylosinus trichosporium* OB3b (C_{0-1} CopC; Lawton *et al.*, 2016), *Escherichia coli* (C_{1-1} CopC; Wernimont *et al.*, 2003) and *Pseudomonas syringae* (C_{1-1} CopC; Zhang *et al.*, 2006) have been determined. In the structures of CopC from *M. trichosporium* and *P. syringae*, the copper(II) ion is coordinated by the N-terminal amino group, His1 N^{δ}, and His N^{δ} and Asp O^{δ} of the conserved His-Xxx-Asp motif. CopCs of the C_{0-2} subfamily are additionally characterized by the presence of a His1-Xxx-His3 motif at the N-terminus (Lawton *et al.*, 2016). The high affinity of C_{0-2} CopCs for copper(II) was confirmed in the study of CopC from *Pseudomonas fluorescens* SBW25 (Wijekoon *et al.*, 2015). The structure of C_{0-2} CopCs remains unknown. The higher affinity of C_{0-2} CopCs for copper(II) has been attributed to the formation of a His3 N^{δ}–copper(II) coordination bond instead of the Asp O^{δ}–copper(II) bond (Wijekoon *et al.*, 2015; Lawton *et al.*, 2016).

An amino-acid sequence alignment and analysis of CopC proteins from different subfamilies showed that the CopC gene from *T. paradoxus* ARh 1, which is located in the operon that also contains the CopD gene, produces a C_{0-2} CopC. In this study, we determined the structure of FCC in complex with this C_{0-2} CopC [*Tp*FCC–(*Tp*CopC)$_2$].

2. Materials and methods

2.1. Protein isolation and purification

T. paradoxus ARh 1 was grown in batch mode on a mineral sodium carbonate–sodium bicarbonate medium containing

0.6 *M* total Na^+ at pH 9.75 as described previously (Sorokin *et al.*, 2001) with sodium thiocyanate (10 m*M*) as an energy and nitrogen source. After the consumption of the thiocyanate, additional 10 m*M* thiocyanate was added. The Cu^{2+} concentration in the growth medium was 30 µg l^{-1}.

After full utilization of the thiocyanate, the cells from a 10 l culture were collected by centrifugation at 6000 rev min^{-1} for 20 min at 4°C, resuspended in approximately 100 ml of the medium, pelleted again at 6000 rev min^{-1} and finally washed with 20 m*M* MOPS buffer pH 7.5 containing 0.6 *M* NaCl. The wet weight of the cells was 21 g.

To obtain the periplasmic fraction, the cells were incubated for 10 min in 42 ml lysis buffer (20 m*M* MOPS pH 7.5, 1 mg ml^{-1} lysozyme, 500 m*M* sucrose) at room temperature. Milli-Q water (63 ml) and 1 m*M* PMSF were then added and incubation was continued at 4°C for 15 min. Spheroplasts and cell debris were separated from the periplasmic fraction by centrifugation at 8000 rev min^{-1} for 30 min.

The periplasmic fraction, as a source of *Tp*FCC, was immediately applied onto a DEAE-Sepharose FF column equilibrated with 50 m*M* MOPS buffer pH 7.5 and eluted with a gradient of 15–70% 1 *M* NaCl in 50 m*M* MOPS buffer pH 7.5. Fractions containing *Tp*FCC were combined, diluted and applied onto a Mono Q 10/100 anion-exchange column (GE Healthcare, USA) equilibrated with 50 m*M* Tris buffer pH 7.5. The proteins were eluted with a gradient of 0–100% 1 *M* NaCl in 50 m*M* Tris buffer pH 7.5.

Fractions containing *Tp*FCC were collected, pooled and applied onto a Superdex 200 10/300 gel-filtration column (GE Healthcare, USA) equilibrated with 50 m*M* Tris buffer pH 7.5, 200 m*M* NaCl. The buffer for isolation and subsequent crystallization was chosen based on the results of thermofluorescence analysis (see below). An ÄKTA FPLC system (GE Healthcare, USA) was used for the runs.

The molecular weight of *Tp*FCC in solution was determined by size-exclusion chromatography on a Superdex 75 10/300 column equilibrated with 50 m*M* Tris buffer pH 7.5, 200 m*M* NaCl. The column was calibrated using molecular-mass standards for size-exclusion chromatography (GE Healthcare, USA).

Finally, the protein was concentrated to 40 mg ml^{-1} and used for crystallization. The protein concentration was determined by the Bradford assay (Bradford, 1976). The purity of the fractions was analyzed by SDS–PAGE according to Laemmli (1970). Identification of proteins was carried out by MALDI-TOF MS using an Ultraflex III MALDI-TOF/TOF mass spectrometer (Bruker, Germany).

2.2. Enzyme-activity assay

The enzyme activity of *Tp*FCC was measured by spectrophotometry in a temperature-controlled cell at 25°C using a Cary 100 Bio spectrometer (Thermo Scientific Varian, USA). The reaction mixture (1 ml) was composed of 50 m*M* glycine buffer pH 9.5, 10 µ*M* sodium sulfide and 14 n*M* enzyme; 20 µ*M* horse heart cytochrome *c* (Sigma, USA) was used as an electron acceptor. The reaction was initiated with sulfide. The reaction rate was calculated from the change in the absorbance of reduced cytochrome *c* at 550 nm (ε_{550} = 22 500 M^{-1} cm^{-1}) in the presence and absence of the enzyme.

Table 1
Data-collection and refinement statistics.

Values in parentheses are for the outer shell.

Data collection	
Space group	$P2_12_12_1$
Unit-cell parameters (Å)	a = 39.5, b = 138.4, c = 155.8
Resolution (Å)	29.76–2.60 (2.70–2.60)
$\langle I/\sigma(I)\rangle$	11.4 (2.1)
$CC_{1/2}$ (%)	99.7 (78.5)
Completeness (%)	99.7 (99.8)
Measured reflections	151142 (15674)
Unique reflections	27206 (2841)
Multiplicity	5.5
R_{meas}† (%)	3.5
Refinement	
R_{cryst} (%)	18.6 (32.0)
R_{free} (%)	25.7 (38.6)
R.m.s.d. from ideal values	
Bond lengths (Å)	0.013
Bond angles (°)	1.9
Average B factors (Å^2)	
Protein	56.8
FAD and haem	46.0
Water	47.5
Copper	82.6
No. of Ramachandran plot outliers	2

† R_{meas} for the inner shell (29.76–7.86 Å).

2.3. Thermofluorescence analysis

The buffer for the final steps of isolation and crystallization was chosen by thermofluorescence analysis (Ericsson *et al.*, 2006) in 96-well PCR plates using a FRET-based MyIQ RT-PCR (Bio-Rad, USA). Each well contained 7.5 µl of 300× SYPRO Orange (Thermo Fisher, USA), 5 µl deionized water, 12.5 µl buffer solution and 12.5 µl protein solution at 1 mg ml^{-1}. The negative control contained 12.5 µl water instead of the protein solution. The samples were heated from 20 to 90°C at a rate of 1°C min^{-1} and the fluorescence yield was measured. To obtain the temperature midpoint for the protein-unfolding transition (T_m), the Boltzmann model was used to fit the fluorescence imaging data (Ericsson *et al.*, 2006). A higher T_m corresponds to higher protein stability in a given buffer.

2.4. Crystallization

Crystallization conditions were screened with a Rigaku Phoenix + Crystal Trak + Gallery 700 system (Rigaku, Japan) using the commercial crystallization screens Index and Crystal Screen (Hampton Research, USA). The crystallization conditions were optimized using the hanging-drop vapour-diffusion technique at 298 K. The drops were composed of equal volumes (1 µl) of protein solution and reservoir solution. Small red needle-like crystals were obtained in a mixture consisting of 0.056 *M* sodium phosphate monobasic monohydrate, 1.344 *M* potassium phosphate dibasic pH 8.2. After manual optimization of the crystallization conditions,

needle-like crystals (200 × 30 × 30 µm) were obtained in 0.2 *M* NaH_2PO_4, 1.3 *M* K_2HPO_4 pH 8.2.

2.5. X-ray data collection and structure determination

X-ray diffraction data sets were collected at 100 K on the ID23-1 beamline at the European Synchrotron Radiation Facility, Grenoble, France using a PILATUS 6M detector (Dectris, Switzerland) at a wavelength of 0.97 Å. Prior to data collection, the crystals were soaked in reservoir solution supplemented with 20%(*v*/*v*) glycerol and then flash-cooled in liquid nitrogen. The data-collection strategy was optimized using the *BEST* program (Bourenkov & Popov, 2010) as incorporated within the *MXCuBE* interface (Gabadinho *et al.*, 2010). The X-ray data sets were processed and merged with *XDS* (Kabsch, 2010). Data-collection statistics are summarized in Table 1.

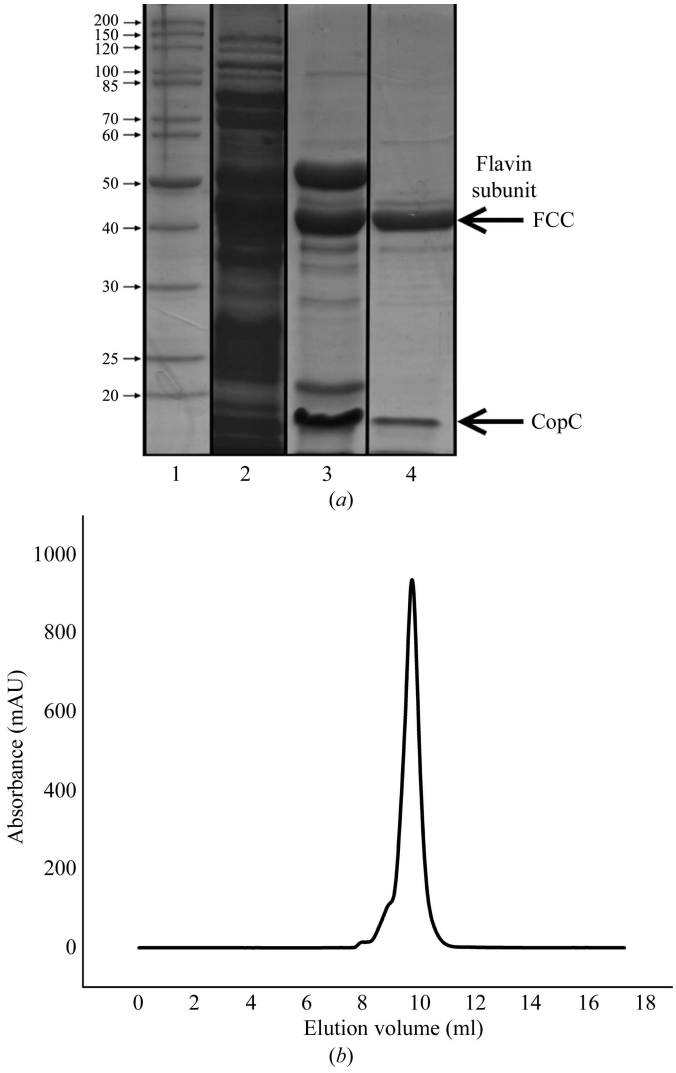

Figure 1
(*a*) SDS–PAGE (12%) of the FCC-containing fractions at different steps in purification. The lanes contain (from left to right) molecular-weight markers (labelled in kDa) and fractions after DEAE-Sepharose, Mono Q and size-exclusion chromatography. The cytochrome *c* subunit of *Tp*FCC is not shown. (*b*) Size-exclusion chromatography of *Tp*FCC–(*Tp*CopC)$_2$ on Superdex 75 10/300. The peak corresponds to a mass of 82 kDa.

The structure of *Tp*FCC was solved by the molecular-replacement method with *MOLREP* (Vagin & Teplyakov, 2010) using the heterodimeric *Av*FCC structure (PDB entry 1fcd; Chen *et al.*, 1994) as the starting model. Structure refinement without solvent molecules and CopC converged to an *R* factor of about 38%, and positive density blobs (>5σ) were visible in difference electron-density maps. After several cycles of polyalanine chain tracing with *Buccaneer* from the *CCP*4 suite (Winn *et al.*, 2011) followed by manual removal of incorrectly placed residues, six β-sheets and two α-helices were found. Based on the β-sheet structure, we identified the position and orientation of *Tp*CopC in the asymmetric unit. β-Sheets of *Tp*CopC were connected based on the alignment of *Tp*CopC with CopC from *P. syringae* (PDB entry 2c9p; Zhang *et al.*, 2006). The structure was refined with *REFMAC*5 (Murshudov *et al.*, 2011). Visual inspection and manual rebuilding of the model were performed with *Coot* (Emsley *et al.*, 2010). Figures were prepared with *PyMOL* (Schrödinger). The structure was deposited in the Protein Data Bank as PDB entry 5n1t.

2.6. Bioinformatics tools

The solvent-accessible surface area was calculated in *PyMOL* using the *get_area* function. H atoms were added to the structure and the molecular weight was calculated using *PyMOL*. The theoretical molecular weight was calculated

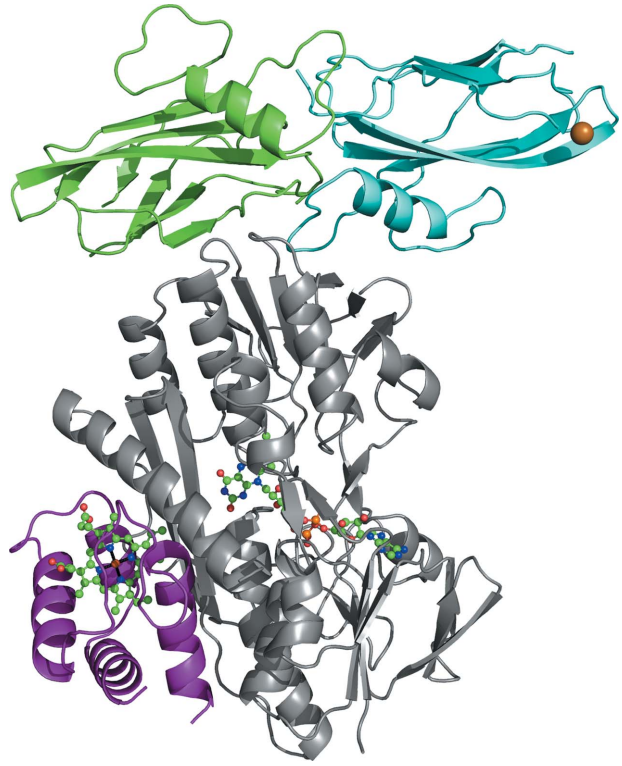

Figure 2
Overall view of the *Tp*FCC–(*Tp*CopC)$_2$ heterotetramer. The flavin-binding subunit is shown in grey, the cytochrome subunit in purple and the two CopC monomers in green (chain *M*) and cyan (chain *W*). The copper ion is represented by an orange sphere. The haem *c* and FAD are shown as ball-and-stick models.

from the amino-acid sequence with *ProtParam*. The presence of a signal peptide in the amino-acid sequences was analyzed using the *SignalP* 4.1 server (Nielsen, 2017). Analysis of intermolecular contacts was performed with *PISA* (Krissinel & Henrick, 2007) and *STRING* (http://string-db.org). The sequence alignment and analysis were performed with *BLAST*. The sequence alignment was visualized with *TEXshade*/*LaTeX*. The surface charge was calculated using the *PyMOL APBS* plugin (Baker *et al.*, 2001). The OMIT map for the CopC dimer was generated in *phenix.polder* (Liebschner *et al.*, 2017)

3. Results and discussion

3.1. Isolation and crystallization of the *Tp*FCC–(*Tp*CopC)$_2$ complex

The complex of *Tp*FCC with the copper-binding protein *Tp*CopC was isolated from a periplasmic fraction of *T. paradoxus* ARh 1 cells grown with thiocyanate as the electron donor and nitrogen source. The localization of the components of the complex in the periplasm is consistent with the data from a bioinformatics analysis, according to which all three subunits of the complex contain a twin-arginine translocation motif (Palmer & Berks, 2012) enabling transport of these subunits across the cytoplasmic membrane to the periplasm. Further purification was accomplished using two anion-exchange and size-exclusion chromatography steps. According to size-exclusion chromatography, the complex has a molecular weight of 82 kDa. SDS–PAGE analysis (Fig. 1*a*) and MALDI-TOF mass spectrometry showed that this complex is composed of the two subunits of FCC, flavin-binding (WP_006748978, molecular weight 42 kDa) and cytochrome (WP_006748977, molecular weight 7.8 kDa), and a protein of the CopC family (WP_006748989, molecular weight 14 kDa; in all cases the calculated molecular weights of mature proteins without a signal peptide are given). Taking into account the molecular weights of the components involved in the complex, the following stoichiometry can be proposed for the complex: 1 *Tp*FCC (heterodimer):2 *Tp*CopC.

A Thermofluor assay was used to optimize the protein buffer prior to crystallization. The Thermofluor assay showed that *Tp*FCC is most stable in 50 m*M* Tris buffer pH 7.5–8.0. Hence, the final size-exclusion chromatography step was performed in 50 m*M* Tris buffer pH 8.0 supplemented with 200 m*M* NaCl.

After size-exclusion chromatography, the sample composed of *Tp*FCC and *Tp*CopC was crystallized. An X-ray diffraction data set was collected to 2.6 Å resolution (Table 1).

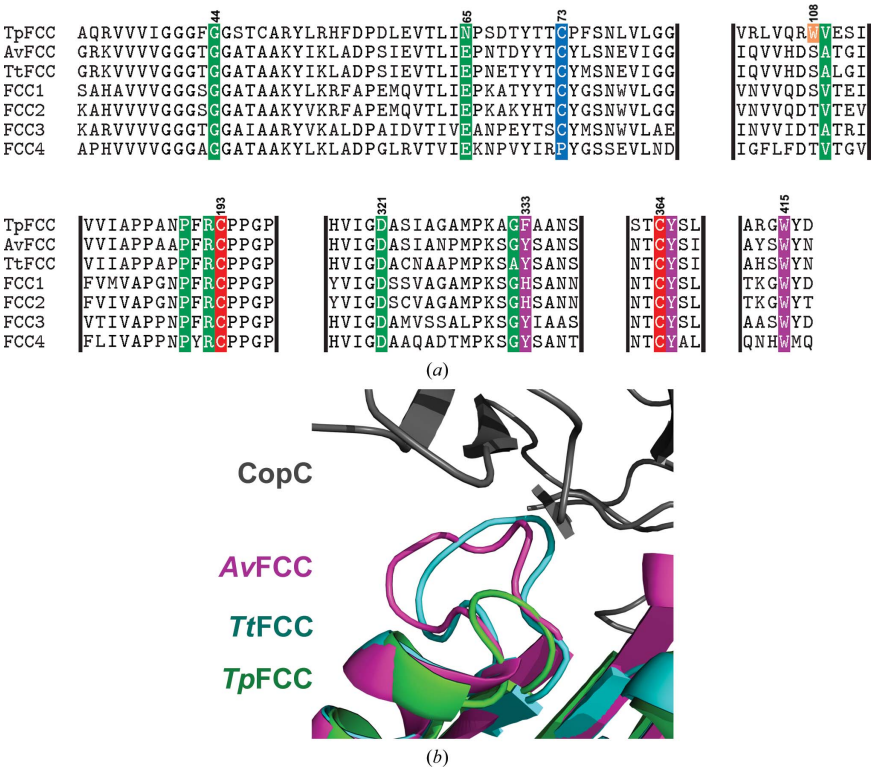

Figure 3
(*a*) Fragments of the multiple sequence alignment of the flavin subunits of FCC from *T. paradoxus* (*Tp*FCC), *A. vinosum* (*Av*FCC) and *T. tepidum* (*Tt*FCC) and the translated sequences of four other FCC genes from the *T. paradoxus* genome (FCC1–FCC4). Redox-active cysteines are highlighted in red, the residues involved in hydrogen bonding to FAD in green, the residues involved in the electron-transport chain from FAD to the haem in purple, the cysteine forming a covalent bond with FAD in blue and Trp108 in orange. Gaps are marked by three dots. (*b*) The loop at the *Tp*FCC–*Tp*CopC interface that adopts different conformations in *Av*FCC, *Tt*FCC and *Tp*FCC.

3.2. Overall structure of the *Tp*FCC–(*Tp*CopC)$_2$ complex

The *Tp*FCC–(*Tp*CopC)$_2$ structure was solved and refined to 2.6 Å resolution. The crystal contains one heterotetramer per asymmetric unit (Fig. 2). There are two Ramachandran plot outliers: Glu67 and Phe75. Both of these are not true outliers and are attributed to the fact that the refinement was performed without Ramachandran plot restraints, as well as the relatively low resolution. The heterotetramer consists of the flavin-binding (chain *A*) and cytochrome (chain *B*) subunits of *Tp*FCC and a homodimer of the *Tp*CopC protein (chains *M* and *W*). The linear dimensions of the protein molecule are 80 × 100 × 50 Å. The flavin-binding subunit contains covalently bound FAD. The single-domain cytochrome subunit contains one covalently bound haem *c*. One of the *Tp*CopC monomers contains a coordinated copper ion.

3.3. Structure of the flavin subunit

The *Tp*FCC subunit shares about 50% primary-structure identity with the flavin-binding subunits of *Av*FCC and *Tt*FCC (Fig. 3) and contains 429 residues, 392 of which

were refined. The first 37 residues are not visible in the electron-density maps. The *Tp*FCC structure superimposes on those of *Av*FCC and *Tt*FCC with C^{α} r.m.s.d.s of 0.8 Å (326 C^{α} atoms) and 0.7 Å (319 C^{α} atoms), respectively. The largest differences between *Tp*FCC and two other FCC structures are observed in the interface region between the flavin-binding subunit and *Tp*CopC in *Tp*FCC (Fig. 3*b*).

The flavin-binding subunit of *Tp*FCC contains six cysteine residues, three of which play a functional role. Thus, Cys73 forms a covalent bond with FAD, while Cys193 and Cys364 form a redox-active pair in the active site (Fig. 4*a*). The functions of the other Cys residues (Cys48, Cys301 and Cys342) are unclear. Cys301 is conserved in all structurally characterized FCCs and is located at a distance of 19 Å from the active site on the surface of the protein molecule, with its side chain buried inside the protein molecule. Cys48 and Cys342 are nonconserved and are only present in the *Tp*FCC structure. These residues are spatially close to each other and are located at the contact interface between two α-helices, but a disulfide bond is not formed between these residues (the Cys48 S^{δ}–Cys342 S^{δ} distance is 4.2 Å).

The environment of the putative sulfide-binding site on the *re* side of FAD is similar in all FCC structures. It can be stated that the binding and oxidation of the sulfide ion in all FCCs proceeds by the same mechanism. Calculations with the *APBS* plugin show that the surface of the flavin subunit in the sulfide-binding region has a positive charge (Fig. 5). The conserved catalytic redox-active residues Cys193 and Cys364 are located directly above the plane of the isoalloxazine ring of FAD (Figs. 4*a* and 4*c*). The shortest distance from the plane of the isoalloxazine ring to the nearest S^{γ} atom of Cys193 is 3.5 Å. The distance between the S^{γ} atoms of Cys193 and Cys364 is 5.4 Å, which is substantially longer than the length of a disulfide bond (2.2 Å). The $F_o - F_c$ electron-density difference map also showed a large positive peak between these atoms. Therefore, Cys193 was replaced with *S*-mercaptocysteine (Css; Fig. 4*c*). After refinement, the distance from the S^{δ} atom of Css193 (orange sphere in Fig. 4*a*) to Cys364 S^{γ} was 2.7 Å. Bound sulfur was found in the active sites of the sulfide dehydrogenases *Tt*FCC (S_2; Hirano *et al.*, 2012) and SQR from *A. aeolicus* (S_8; Marcia *et al.*, 2009). Cys193 was supposed to act as a nucleophilic agent and to be involved in electron transfer to bound FAD (Cherney *et al.*, 2010, 2012). Electron transfer to FAD is accompanied by the oxidation of Cys193 S^{γ}, resulting in the formation of a disulfide bond with the substrate.

The fold of the part of the flavin-binding subunit that is responsible for the binding of FAD is conserved among all FCC structures. It should be noted that FAD adopts a

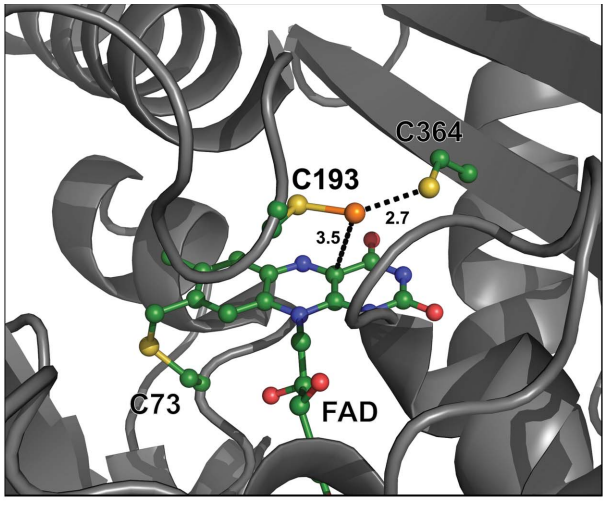

(*a*)

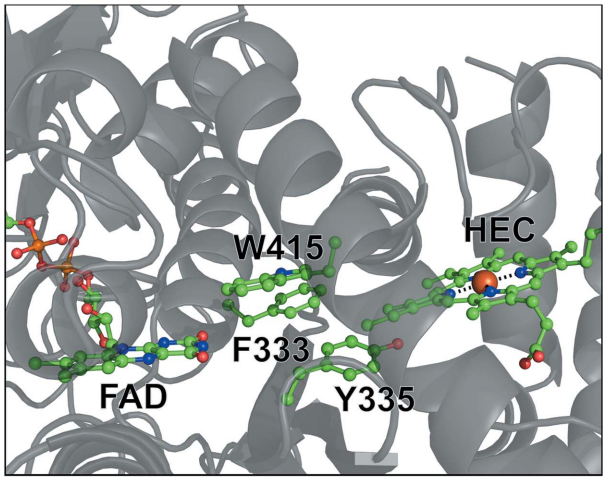

(*b*)

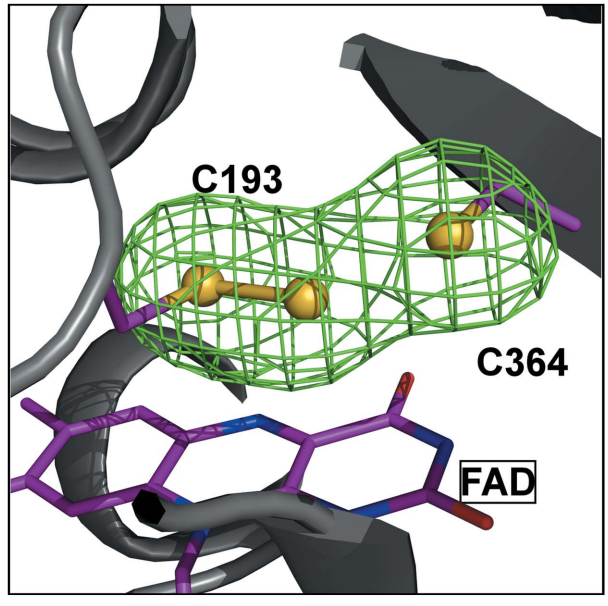

(*c*)

Figure 4
(*a*) Functionally significant cysteine residues: Cys73 covalently bound to FAD and the redox-active pair Cys193–Cys364. Cys193 is linked to the S atom of the substrate (orange sphere). The distances between the atoms are shown by dashed lines labelled in Å. (*b*) The π-conjugated electron-transport system from FAD to the haem (HEC). The residues involved in the π-conjugated system are shown as ball-and-stick models. (*c*) 5σ $F_o - F_c$ OMIT map (green mesh) for S atoms (yellow spheres) in the active site of *Tp*FCC.

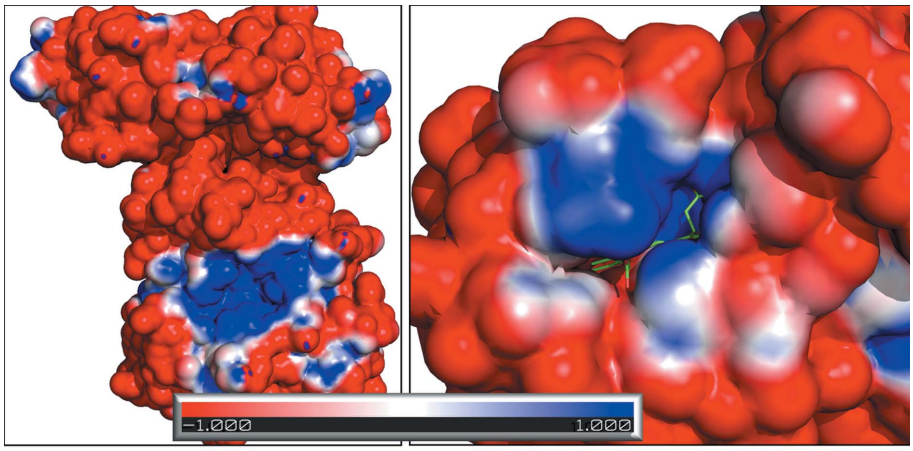

(*a*) (*b*)

Figure 5
(*a*) Electrostatic surface potential of the flavin-binding subunit of *Tp*FCC calculated using the *PyMOL APBS* plugin. The large blue surface patch corresponds to the entrance to the sulfide-binding site. (*b*) Electrostatic surface potential of the cytochrome subunit of *Tp*FCC in the region where the haem is exposed to the solvent. The haem is shown as a stick model.

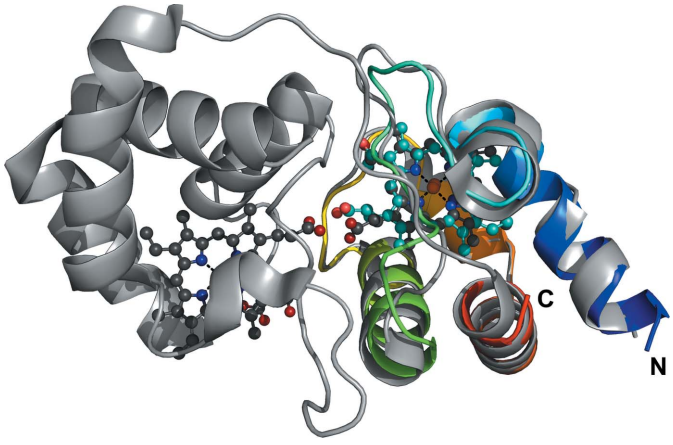

Figure 6
Cartoon representation of the cytochrome subunit of *Tp*FCC (rainbow-coloured) aligned with the first domain of the dihaem subunit of *Tt*FCC (grey). The haem groups are shown as ball-and-stick models. Haem iron is shown as an orange sphere.

somewhat different conformation in *Tp*FCC and *Av*FCC. In the *Tp*FCC and *Tt*FCC structures the pentoxy moiety of the FAD molecule adopts the proper configuration (2*R*,3*S*,3*S*), while in the AvFCC structure this moiety has the inverse configuration (2*S*,3*R*,3*R*). The FAD molecule is covalently bound to the protein by the FAD C8a–Cys73 S^{γ} thioether bond (1.7 Å). Cys73 is conserved in all FCC structures and is replaced by proline in SQR structures, in which the FAD molecule is bound noncovalently. The conformation of FAD is stabilized by eight hydrogen bonds. Most of the residues that are involved in these hydrogen bonds are conserved in all known FCC structures: Gly44, Val109, Pro190, Arg192, Asp321, Gly332 and Phe333 (the numbering corresponds to the *Tp*FCC structure).

Despite the conservation of the polypeptide chain fold around FAD, there are substitutions of some functional residues in the *Tp*FCC structure. Glu36, which forms a hydrogen bond to the ribose O3 atom of FAD in *Av*FCC and *Tt*FCC, is replaced by Asn65 in *Tp*FCC. Of the five copies of the gene for FCC in the *T. paradoxus* genome, only *Tp*FCC as characterized in this study contains asparagine at this position; the other copies of the gene for FCC in the *T. paradoxus* genome contain a glutamic acid residue (FCC1–FCC4 in Fig. 3). The *Tp*FCC structure contains Pro74 on the *si* side of the isoalloxazine ring of FAD, which corresponds to Tyr43 in *Tt*FCC and *Av*FCC. The other copies of the FCC gene in the *T. paradoxus* genome contain tyrosine at this position. Therefore, the environment of the FAD molecule in the *Tp*FCC structure differs from that in the other structurally characterized FCC, as well as from the other four copies of FCC from the *T. paradoxus* genome.

In *Tp*FCC FAD is less solvent-accessible compared with *Av*FCC and *Tt*FCC owing to shielding of the adenine group of FAD by the side group of Trp108. The shortest distance from the indole ring of Trp108 (the $C^{\zeta 3}$ atom) to the plane of the purine ring of FAD is 3.3 Å, thus preventing a water molecule from approaching the purine ring of FAD. This shielding results in a decrease in the solvent-accessible surface area of FAD by 200 $Å^2$.

The aromatic groups of FAD, Phe333, Tyr365 and Trp415 of the flavin-binding subunit and the haem of the cytochrome subunit are coplanar and form an extended π-interaction system (Fig. 4*b*). This coplanar π–π system is conserved and forms a potential electron-transport chain from FAD to the haem of the cytochrome subunit in all FCC structures. In the other copies of the FCC gene Phe333 is replaced by tyrosine or histidine, *i.e.* by a residue containing an aromatic side chain that is capable of being involved in π–π interactions.

3.4. Cytochrome *c* subunit of *Tp*FCC

The cytochrome subunit of FCC (chain *B*) is composed of 75 residues arranged as four α-helices (Fig. 6). The polypeptide chain fold is similar to those in the N-terminal domains of the two-domain cytochrome subunits of *Av*FCC and *Tt*FCC. The sequence identity and r.m.s.d. between equivalent C^{α} atoms are 40% and 0.82 Å (67 C^{α} atoms), respectively, for *Tt*FCC, and 40% and 0.98 Å (68 C^{α} atoms), respectively, for *Av*FCC.

The Fe atom of haem *c* is hexacoordinated by His15 N^{ϵ} and Met53 S^{δ} in axial positions. The position of the imidazole ring of His15 is stabilized by a His15 $N^{\delta}\cdots$Pro26 O hydrogen bond. One propionate group of the haem is exposed to the solvent, while another is covered by the polypeptide chain (the Ser45–Met53 loop).

The most substantial difference between the *Tp*FCC and the *Tt*FCC and *Av*FCC structures is that *Tp*FCC contains a haem *c*-binding domain. In the dihaem structures of *Tt*FCC and *Av*FCC the propionate groups of the two haems are buried at the interdomain interface of the two-domain cytochrome *c* and are linked to each other by hydrogen bonds. In contrast, one propionate group of haem *c* in *Tp*FCC is exposed to the solvent. In *Tp*FCC the haem solvent accessibility is ∼300 Å^2 higher than those of both haems *c* in other FCC structures (the total surface area of the haem is 1434 Å^2).

The surface of the cytochrome subunit is predominantly negatively charged and bears a positive charge in the region where the haem is exposed to the solvent (Fig. 5*b*), which is the most probable binding site for the electron acceptor.

3.5. Structure of the copper-binding protein *Tp*CopC

Structure refinement of the *Tp*FCC heterodimer converged to *R* factors of ∼38%. The difference electron-density maps showed large peaks (>5σ) at distances of greater than 10 Å from the nearest polypeptide chain. After fitting of the *Tp*CopC dimer to this density and subsequent refinement, the *R* and $R_{\rm free}$ factors decreased to 18 and 25%, respectively.

The crystal structure contains one *Tp*CopC homodimer per asymmetric unit (Fig. 7*a*). Residues His1–Thr127 (chain *M*) and His1–Gly125 (chain *W*) were located in electron-density maps. The C-termini of these chains are disordered; six (chain *W*) and four (chain *M*) residues were not observed in the electron-density maps. Residues 81–83 in chain *M* and Ser81 in chain *W* were also not visible. These disordered residues are located in the Asp79–Gln83 loop at a distance of 15 Å from the copper-binding site. We attributed the absence of electron density for residues 81–83 in chain *M* to conformational rearrangements upon dissociation of the copper(II) ion from the copper-binding site (see below).

The *Tp*CopC monomer consists of two four-stranded β-sheets and one α-helix. The β-sheets form a sandwich structure. Leu52–Glu61 form an α-helix which lies on the external surface of one of the β-sheets and is stabilized by three intramolecular hydrogen bonds. The α-helix Leu52–Glu61 is a distinguishing feature of *Tp*CopC and is not present in the other structurally characterized CopC (Fig. 7*c*). The α-helix of chain *W* is located at the intermolecular interface between *Tp*CopC and the flavin-binding subunit of *Tp*FCC (chain *A*). Therefore, the α-helix apparently plays a key role in formation of the *Tp*FCC–(*Tp*CopC)$_2$ complex.

*Tp*CopC has a His1-Xxx-His3 motif at the N-terminus and belongs to the C_{0-2} CopC subfamily (Lawton *et al.*, 2016). This subfamily is characterized by the presence of one high-affinity copper(II)-binding site per subunit. It has been proposed that it is His3 that provides the high binding affinity of C_{0-2} CopC for copper(II) ions owing to the replacement of asparagine in the coordination sphere of the copper ion (Lawton *et al.*, 2016; Wijekoon *et al.*, 2015).

In *Tp*CopC, chain *W* binds one copper(II) ion in the active site at the N-terminus (Fig. 7*b*). This copper ion has a square-planar geometry and is coordinated by the N-terminal amino group, His1 N$^{\delta}$, Asp110 O$^{\delta}$ and His112 N$^{\delta}$. A similar geometry of the coordination environment of the copper(II) ion has been observed in other known CopC structures. His3 is not involved in copper binding and is located at a distance of 6–7 Å from the copper(II)-binding site. Therefore, the presence of the His1-Xxx-His3 motif is not responsible for the high affinity of C_{0-2} CopC for copper(II) ions. The main difference in the copper-binding site in *Tp*CopC is that the amino group of His1 forms an additional His1 N$\cdots$Glu28 O$^{\varepsilon}$ hydrogen bond. In the structure of CopC from *P. syringae* (Zhang *et al.*, 2006) the His1 N–Glu27 O$^{\varepsilon}$ distance is 4.2 Å, *i.e.* this hydrogen bond is absent. Apparently, the hydrogen bond between His1 N and Glu28 O$^{\varepsilon}$ is responsible for the higher affinity of C_{0-2} CopC for copper(II) ions owing to an increase in the nucleophilicity of the amino group of His1.

In chain *M* the copper-binding site is unoccupied. Metal-containing proteins are known to undergo photoreduction under X-ray irradiation (De la Mora *et al.*, 2012; Antonyuk & Hough, 2011; Bowman *et al.*, 2016). Therefore, we attributed the absence of copper in chain *M* to the photoreduction of copper(II) to copper(I) followed by dissociation of copper(I) from the copper-binding site. The absence of a copper ion causes the difference in the structures of chains *M* and *W*. The *Tp*CopC monomers superimpose with an r.m.s.d. of 0.4 Å over 334 equivalent C$^{\alpha}$ atoms. The most substantial difference in the spatial arrangement of the monomers is observed in the Val109–His112 loop that is involved in the coordination of the copper ion.

The fact that the copper(II) ion is predominantly reduced in chain *M* of *Tp*CopC may be associated with the crystal packing of *Tp*FCC–(*Tp*CopC)$_2$. Chain *M* of *Tp*CopC forms an intermolecular contact with the cytochrome subunit of the symmetry-related *Tp*FCC–(*Tp*CopC)$_2$ molecule. His1 of chain *M* is at a distance of ∼14 Å from the haem of this cytochrome. The short distance ensures electron transfer from the closely located haem as a source of electrons to the copper-binding site of chain *M* as an electron acceptor.

3.6. Intersubunit contacts in the *Tp*FCC–(*Tp*CopC)$_2$ heterotetramer

There are strong contacts between the flavin and cytochrome subunits of the functional *Tp*FCC heterodimer and between the *Tp*CopC monomers. All of the FCCs described in the literature exist as stable heterodimers and all CopCs form stable homodimers.

Complexes of FCC with CopC have not been described previously. The interface between *Tp*FCC and *Tp*CopC is located far (>20 Å) from the residues that are essential for sulfide oxidation. In *Tp*CopC the interface with *Tp*FCC is also far from the copper-binding sites. Therefore, *Tp*CopC is not a component of the sulfide-oxidizing machinery and *Tp*FCC is not directly involved in copper binding.

Contacts between the flavin-binding subunit and individual *Tp*CopC monomers are weak. The interface between the CopC dimer and the flavin subunit is stabilized by seven hydrogen bonds and four salt bridges (Fig. 8). The following

four residues are involved in salt bridges: Arg214 and Arg271 of the flavin-binding subunit of *Tp*FCC and Glu11 of chain *M* and Glu61 of chain *W* of the *Tp*CopC dimer. Glu61 belongs to the α-helix of *Tp*CopC.

In *Tp*CopC, the residues forming salt bridges are located inside the α-helix. This α-helix was not observed in the CopC structures described previously and is not directly associated with the copper-binding function. Apparently, this α-helix is required for interactions with other proteins and can be considered to be a hallmark of the CopC subfamily.

The free energy of dissociation of *Tp*FCC and *Tp*CopC is close to zero, although *PISA* scores this complex as nonstable. This means that the complex is rather unstable and dissociates under standard conditions. The crystallization conditions (1.3 *M* phosphate pH 8.2), which slightly resemble the typical environment in the periplasm of haloalkaliphilic bacteria (2 *M* ionic strength, pH 10), and the high protein concentration used for crystallization (40 mg ml^{-1}) probably shift the equilibrium towards formation of the *Tp*FCC–(*Tp*CopC)$_2$ complex.

3.7. Putative biological function of the *Tp*FCC–(*Tp*CopC)$_2$ complex

The biological function of the *Tp*FCC–(*Tp*CopC)$_2$ complex is unclear. In the genome, the gene cluster encoding *Tp*FCC is present at a distance of ten genes or 14 000 bp from that encoding *Tp*CopC. A search for biological partners of *Tp*FCC and *Tp*CopC using *STRING* did not reveal interactions between them.

We can speculate as to how *Tp*FCC and *Tp*CopC form a complex. It was hypothesized that together the CopC and CopD proteins are responsible for the incorporation of copper into fully folded copper-containing proteins in the cytoplasm

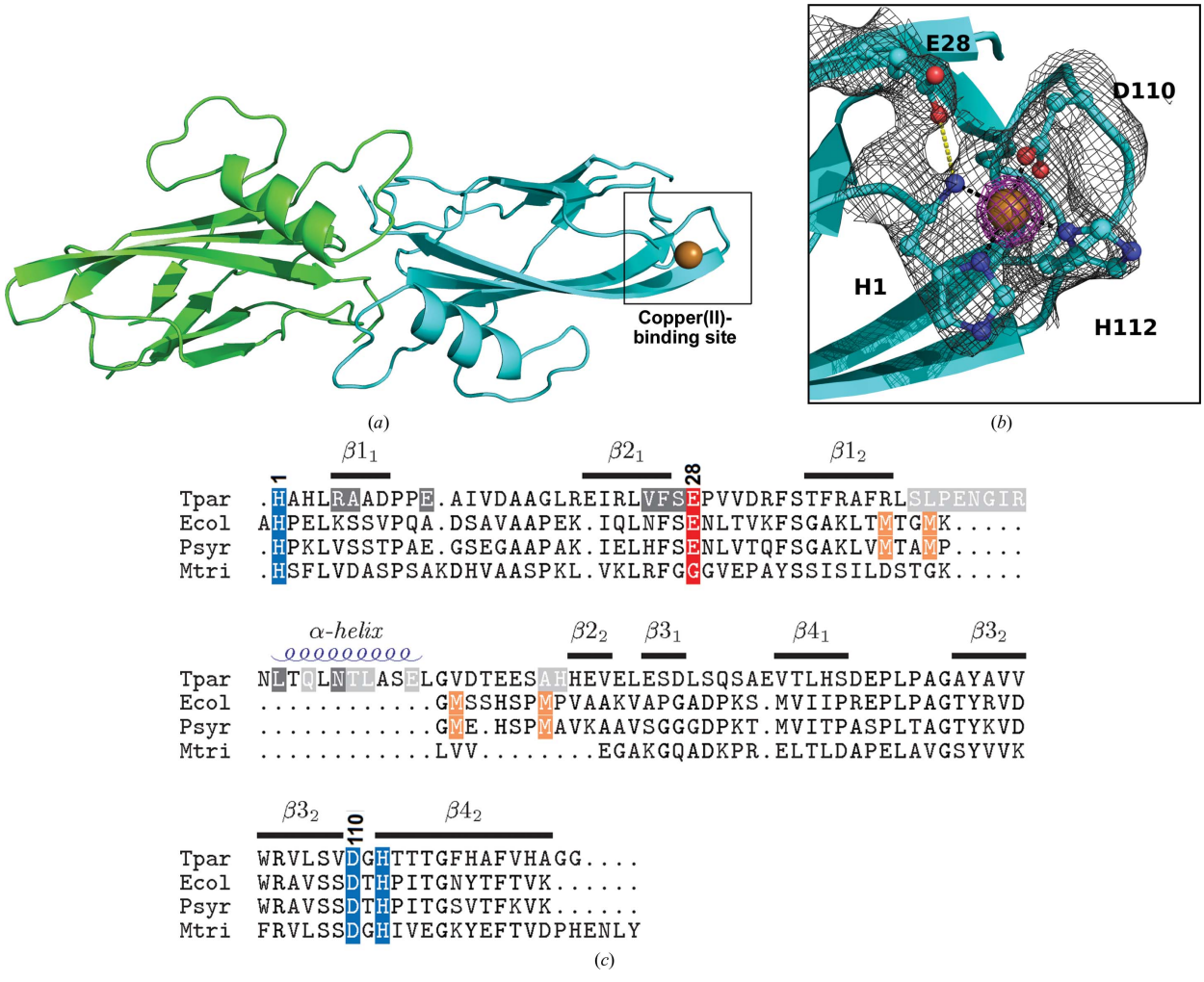

Figure 7
(*a*) Overview of the dimeric *Tp*CopC consisting of chains *M* (green) and *W* (cyan). (*b*) The copper(II)-binding site in chain *W*. The copper ion (orange sphere) has a square-planar coordination formed by His1 N, His1 N$^{\delta}$, Asp110 O$^{\delta}$ and His112 N$^{\delta}$ (black dashed lines). The His1 N atom forms a hydrogen bond to Glu28 O$^{\varepsilon}$ (yellow dashed line). The $2F_o - F_c$ electron-density map is shown as a mesh at 1σ (grey) and 5σ (purple). (*c*) Alignment of *Tp*CopC (Tpar) and the CopCs from *E. coli* (PDB entry 1lyq; Ecol; Wernimont *et al.*, 2003), *P. syringae* (PDB entry 2c9q; Psyr; Zhang *et al.*, 2006) and *M. trichosporium* (PDB entry 5icu; Mtri; Lawton *et al.*, 2016). The copper(I)-binding site is shown in orange and the copper(II)-binding site is in blue. Glu28 is coloured red. The residues of *Tp*CopC that interact with *Tp*FCC are shown in dark grey (chain *M*) and grey (chain *W*). Secondary-structure elements of *Tp*CopC are depicted above the sequence.

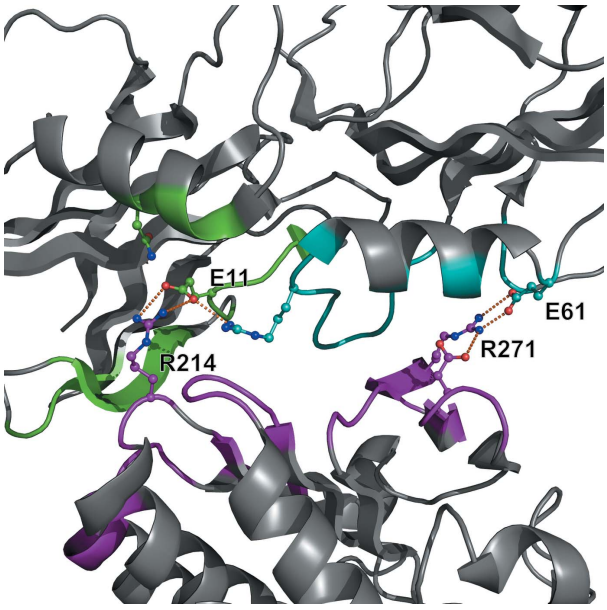

Figure 8
Interface between *Tp*FCC and the *Tp*CopC dimer. Residues involved in the interface formation are coloured cyan (CopC, chain *W*), green (CopC, chain *M*) and purple (*Tp*FCC). Residues involved in salt-bridge formation are shown as ball-and-stick models. Salt bridges are depicted as orange dashed lines.

(Lawton *et al.*, 2016). The gene for periplasmic copper-dependent thiocyanate dehydrogenase (TcDH; PDB entry 5f75, unpublished work) is located directly at the 5′ end of the CopCD operon. Therefore, in the periplasmic space *Tp*CopC may be associated with the thiocyanate-oxidation system as a protein involved in the incorporation of copper ions into TcDH. *Tp*FCC, in turn, may be associated with the metabolism of sulfur produced by the TcDH-catalyzed oxidation of thiocyanate.

Therefore, it can be hypothesized that the *Tp*FCC–(*Tp*CopC)$_2$ heterotetramer, the structure of which is determined in this study, is part of a large periplasmic copper-dependent complex. This complex contains *Tp*FCC, *Tp*CopC and TcDH. The role of the complex is to oxidize thiocyanate and utilize the resulting sulfur.

Acknowledgements

MALDI-TOF MS analysis was carried out with the equipment of the Shared-Access Equipment Centre 'Industrial Biotechnology' of the Federal Research Center 'Fundamentals of Biotechnology' at the Russian Academy of Sciences.

Funding information

This work was supported by the Russian Science Foundation (Project No. 14-24-00172, structure determination and analysis) and the Russian Foundation for Basic Research (Project No. 16-04-01818, protein isolation and crystallization). DYS was supported by RFBR grant 16-04-00035.

References

Antonyuk, S. V. & Hough, M. A. (2011). *Biochim. Biophys. Acta*, **1814**, 778–784.
Baker, N. A., Sept, D., Joseph, S., Holst, M. J. & McCammon, J. A. (2001). *Proc. Natl Acad. Sci. USA*, **98**, 10037–10041.
Berben, T., Sorokin, D. Y., Ivanova, N., Pati, A., Kyrpides, N., Goodwin, L. A., Woyke, T. & Muyzer, G. (2015). *Stand. Genomic Sci.* **10**, 105.
Bourenkov, G. P. & Popov, A. N. (2010). *Acta Cryst.* D**66**, 409–419.
Bowman, S. E. J., Bridwell Rabb, J. & Drennan, C. L. (2016). *Acc. Chem. Res.* **49**, 695–702.
Bradford, M. M. (1976). *Anal. Biochem.* **72**, 248–254.
Brito, J. A., Sousa, F. L., Stelter, M., Bandeiras, T. M., Vonrhein, C., Teixeira, M., Pereira, M. M. & Archer, M. (2009). *Biochemistry*, **48**, 5613–5622.
Chen, Z., Koh, M., Van Driessche, G., Van Beeumen, J., Bartsch, R., Meyer, T., Cusanovich, M. & Mathews, F. (1994). *Science*, **266**, 430–432.
Cherney, M. M., Zhang, Y., James, M. N. G. & Weiner, J. H. (2012). *J. Struct. Biol.* **178**, 319–328.
Cherney, M. M., Zhang, Y., Solomonson, M., Weiner, J. H. & James, M. N. G. (2010). *J. Mol. Biol.* **398**, 292–305.
De la Mora, E., Lovett, J. E., Blanford, C. F., Garman, E. F., Valderrama, B. & Rudino-Pinera, E. (2012). *Acta Cryst.* D**68**, 564–577.
Emsley, P., Lohkamp, B., Scott, W. G. & Cowtan, K. (2010). *Acta Cryst.* D**66**, 486–501.
Ericsson, U. B., Hallberg, B. M., DeTitta, G. T., Dekker, N. & Nordlund, P. (2006). *Anal. Biochem.* **357**, 289–298.
Fukumori, Y. & Yamanaka, T. (1979). *J. Biochem.* **85**, 1405–1414.
Gabadinho, J. *et al.* (2010). *J. Synchrotron Rad.* **17**, 700–707.
Grant, W. D. & Sorokin, D. Y. (2011). *Extremophiles Handbook*, edited by K. Horikoshi, pp. 27–54. Tokyo: Springer.
Hirano, Y., Kimura, Y., Suzuki, H., Miki, K. & Wang, Z.-Y. (2012). *Biochemistry*, **51**, 6556–6567.
Kabsch, W. (2010). *Acta Cryst.* D**66**, 125–132.
Kostanjevecki, V., Brigé, A., Meyer, T. E., Cusanovich, M. A., Guisez, Y. & van Beeumen, J. (2000). *J. Bacteriol.* **182**, 3097–3103.
Krissinel, E. & Henrick, K. (2007). *J. Mol. Biol.* **372**, 774–797.
Laemmli, U. K. (1970). *Nature (London)*, **227**, 680–685.
Lawton, T. J., Kenney, G. E., Hurley, J. D. & Rosenzweig, A. C. (2016). *Biochemistry*, **55**, 2278–2290.
Liebschner, D., Afonine, P. V., Moriarty, N. W., Poon, B. K., Sobolev, O. V., Terwilliger, T. C. & Adams, P. D. (2017). *Acta Cryst.* D**73**, 148–157.
Marcia, M., Ermler, U., Peng, G. & Michel, H. (2009). *Proc. Natl Acad. Sci. USA*, **106**, 9625–9630.
Murshudov, G. N., Skubák, P., Lebedev, A. A., Pannu, N. S., Steiner, R. A., Nicholls, R. A., Winn, M. D., Long, F. & Vagin, A. A. (2011). *Acta Cryst.* D**67**, 355–367.
Nielsen, H. (2017). *Methods Mol. Biol.* **1611**, 59–73.
Palmer, T. & Berks, B. (2012). *Nature Rev. Microbiol.* **10**, 483–496.
Shahak, Y. & Hauska, G. (2008). *Sulfur Metabolism in Phototrophic Organisms*, edited by R. Hell, C. Dahl, D. Knaff & T. Leustek, pp. 319–335. Dordrecht: Springer.
Sorokin, D. Y., Banciu, H., Robertson, L. A., Kuenen, J. G., Muntyan, M. S. & Muyzer, G. (2013). *The Prokaryotes: Prokaryotic Physiology and Biochemistry*, edited by E. Rosenberg, E. F. DeLong, S. Lory, E. Stackebrandt & F. Thompson, pp. 529–554. Berlin: Springer.
Sorokin, D. Y., Berben, T., Melton, E. D., Overmars, L., Vavourakis, C. D. & Muyzer, G. (2014). *Extremophiles*, **18**, 791–809.
Sorokin, D. Y., Gorlenko, V. M., Tourova, T. P., Tsapin, A. I., Nealson, K. H. & Kuenen, G. J. (2002). *Int. J. Syst. Evol. Microbiol.* **52**, 913–920.
Sorokin, D. Y., Rusanov, I. I., Pimenov, N. V., Tourova, T. P., Abbas, B. & Muyzer, G. (2010). *FEMS Microbiol. Ecol.* **73**, 278–290.

Sorokin, D. Y., Tourova, T. P., Lysenko, A. M. & Kuenen, J. G. (2001). *Appl. Environ. Microbiol.* **67**, 528–538.
Vagin, A. & Teplyakov, A. (2010). *Acta Cryst.* D**66**, 22–25.
Visser, J. M., de Jong, G., Robertson, L. A. & Kuenen, J. G. (1997). *Arch. Microbiol.* **167**, 295–301.
Wernimont, A. K., Huffman, D. L., Finney, L. A., Demeler, B., O'Halloran, T. V. & Rosenzweig, A. C. (2003). *J. Biol. Inorg. Chem.* **8**, 185–194.
Wijekoon, C. J. K., Young, T. R., Wedd, A. G. & Xiao, Z. (2015). *Inorg. Chem.* **54**, 2950–2959.
Winn, M. D. *et al.* (2011). *Acta Cryst.* D**67**, 235–242.
Zhang, L., Koay, M., Maher, M. J., Xiao, Z. & Wedd, A. G. (2006). *J. Am. Chem. Soc.* **128**, 5834–5850.